



Bilayer stacking ferrovalley materials without breaking time-reversal and spatial-inversion symmetry

Guoliang Yu ^{1,2,*}, Junyi Ji,^{1,2,*} Changsong Xu,^{1,2,†} and H. J. Xiang ^{1,2,3,‡}

¹Key Laboratory of Computational Physical Sciences (Ministry of Education), Institute of Computational Physical Sciences, State Key Laboratory of Surface Physics, and Department of Physics, Fudan University, Shanghai 200433, China

²Shanghai Qi Zhi Institute, Shanghai 200030, China

³Collaborative Innovation Center of Advanced Microstructures, Nanjing 210093, China



(Received 8 June 2023; revised 15 September 2023; accepted 29 January 2024; published 28 February 2024)

Ferrovalley, which refers to the valley polarization being nonvolatile and switchable, is highly desired for valleytronics applications but remains challenging due to rare candidate materials. Here we propose a strategy to realize ferrovalley with bilayer stacking (BSFV) in many candidate systems. As a special case of BSFV, sliding ferrovalley corresponds to the bilayers obtained by a direct AA stacking and subsequent in-plane sliding. Different from previous approaches, the BSFV strategy not only maintains time-reversal symmetry, but also keeps spatial-inversion symmetry in many cases. Importantly, switching of the valley polarization can be easily achieved by interlayer sliding. Group theory analysis is systematically performed over all kinds of lattices to identify those that can host BSFV. High-throughput screening is carried out and leads to 14 BSFV candidates with direct bandgap and 338 with indirect bandgap. First-principles verification of BSFV indicates that the valley polarization can be realized in, e.g., (i) the hexagonal RhCl_3 bilayer with a threefold rotation symmetry and 39 meV energy difference among valleys, and (ii) the square-latticed InI bilayer with a fourfold rotation symmetry and 326 meV energy difference among valleys. The presently proposed BSFV strategy offers a highly convenient approach for the realization of polarizers and the advancement of valleytronics applications.

DOI: [10.1103/PhysRevB.109.075434](https://doi.org/10.1103/PhysRevB.109.075434)

I. INTRODUCTION

Valley in electronic structure refers to the local minima of conduction band or the maxima of the valence band in momentum space. The valleys are usually degenerate, as specific k points can be connected by certain symmetries, such as time-reversal (TR) symmetry and spatial-inversion (SI) symmetry. Removing such valley degeneracy leads to novel applications such as valley-based logic gates, memory devices, and optoelectronics (e.g., light-emitting diodes and photodetectors) [1–5], giving rise to the emerging field of valleytronics [4–9]. Different approaches have been applied to lift valley degeneracy, such as optical pumping [10–12], magnetic field [13–15], and electric field [16]. However, the valley polarizations induced by such stimuli are transient or volatile, which hinders applications in valleytronics.

To facilitate valleytronics applications, it requires the valley polarization to be nonvolatile and switchable among equivalent valleys, i.e., ferrovalley. Two major strategies have been proposed to realize ferrovalley. One strategy is to break the TR symmetry with magnetism, which can be either to place a valley system being proximate with magnetic substrate [17–24], or to adopt two-dimensional (2D) valley polarized semiconductors that intrinsically exhibit magnetism [25–29].

Although such approaches guarantee nonvolatility, the former suffers from poor ability of switching, while the latter is subject to harsh requirements on anisotropy and low critical temperatures of most 2D magnets [30]. Another strategy is to break the SI symmetry with ferroelectricity, where the valley polarization emerges simultaneously with electric polarization and can be easily switched by electric field [31–33]. However, it is challenging to find suitable 2D ferroelectrics with coupled electric polarization and valleys, especially at room temperature [34]. Note that ferrovalley behaviors based on existing mechanisms have not yet been experimentally demonstrated, suggesting that new mechanisms for ferrovalley are highly desirable.

Recently, 2D materials have experienced flourishing development and the stacking of them, e.g., bilayers, is found to be an effective handle to manipulate physical properties. For example, twisted bilayers exhibit diverse electronic properties [35] and sliding bilayers can create ferroelectricity [36–47]. Moreover, a theory of bilayer stacking ferroelectricity was proposed in our recent study [42], which summarizes general rules of the creation and annihilation of symmetries using stacking degree of freedom. Such rules can naturally be applied to remove the valley degeneracy protected by crystalline symmetries, indicating that ferrovalley can be achieved in various bilayers.

In this paper, we propose a concept of bilayer stacking ferrovalley (BSFV), within which the symmetry breaking required by ferrovalley can be realized by changes in stackings. Different from existing paradigms, the BSFV approach does

*These authors contributed equally to this work.

†csxu@fudan.edu.cn

‡hxiang@fudan.edu.cn

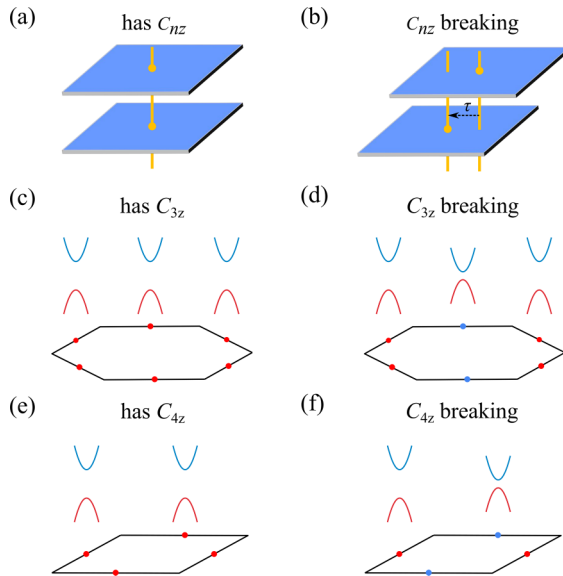


FIG. 1. Illustration of realizing valley polarization through BSFV theory. (a) Schematics of a bilayer with C_{nz} rotational symmetry and (b) breaking of C_{nz} with interlayer sliding τ . (c) Brillouin zone of a hexagonal lattice and degenerate valleys connected by C_{3z} symmetry. (d) Valley polarization realized by breaking C_{3z} with sliding. Red and blue dots represent the positions of degenerate and polarized valley, respectively. Panels (e) and (f) are similar to (c) and (d), respectively, but for square lattice with C_{4z} symmetry.

not require magnetism or ferroelectricity, and thus is not necessary to break TR or SI symmetries. Interestingly, the valley polarization can be switched among different valleys by simply tuning the sliding of bilayers. Our group theory analysis indicates that BSFV can be created with monolayer valley materials that crystallized in hexagonal or square lattices. By screening the material database, we find that fourteen 2D monolayer materials with direct bandgaps are suitable for BSFV. The realization of BSFV (more precisely, sliding ferrovalley here) is further demonstrated in RhCl_3 and InI bilayers by performing first-principles calculations. Both bilayers exhibit switchable ferrovalleys without breaking TR and SI symmetries.

II. DESIGN STRATEGY AND GROUP THEORY ANALYSIS

The basic idea of realizing BSFV is to break the symmetries that map degenerate valleys to each other in the Brillouin zone of a monolayer by means of bilayer stacking [see Figs. 1(a) and 1(b)]. For example, in the hexagonal and square lattices shown in Figs. 1(c) and 1(e), the degenerate valleys are connected to each other through C_{3z} and C_{4z} rotational symmetry operations. However, if these symmetries are broken by bilayer stacking, the valleys can be polarized [see Figs. 1(d) and 1(f)]. We assume that the positions of the valleys in the directly stacked bilayer (with no sliding) is the same as that in single layer, as the interlayer interaction is usually weak.

Now we apply group theory to investigate the valley polarization induced by bilayer stacking. Let us consider that G is the layer group of a monolayer, and one of the

degenerate valleys locates at \mathbf{k} . Applying all the operations g in G to the valley at \mathbf{k} , it will be invariant or transformed into degenerate valleys $\mathbf{k}' = g\mathbf{k}$, since $E(\mathbf{k}) = E(g\mathbf{k})$, where g_c is the connecting symmetry that we aim to break. Note that bilayer stacking can in principle break all point-group symmetries but cannot break TR symmetry. Thus, degenerate valleys connected by TR symmetry at (k_x, k_y) and $(-k_x, -k_y)$, e.g., K and K' in hexagonal lattice, cannot become polarized by bilayer stacking. In the following, we only focus on the degenerate valleys that are not related by TR symmetry.

Then, we investigate the possibilities of realizing BSFV in four types of 2D lattices. (1) In the oblique lattice, all degenerate valleys are connected by TR symmetry [see Sec. 1 of the Supplemental Material (SM) [48]]. (2) In the rectangular lattice, degenerate valleys that are not related by TR symmetry can take place only at general k points (see Sec. 1 of SM), thus we no longer consider the rectangular lattice as here we focus on the case where the valley occurs at high-symmetry lines or points. (3) In the square lattice, fourfold rotations C_{4z} (or improper rotation S_{4z}) can result in valley degeneracy, and the valley polarization can be generated by breaking C_{4z} (or S_{4z}) in this case [see Figs. 1(e) and 1(f)]. (4) In the hexagonal lattice, threefold rotations C_{3z} can result in valley degeneracy at \mathbf{k} , $C_{3z}\mathbf{k}$, and $C_{3z}^2\mathbf{k}$, where the valley polarization can be induced by breaking C_{3z} [see Figs. 1(c) and 1(d)]. According to the group theory analysis on bilayer stacking in Ref. [42], C_{nz} and S_{nz} can always be broken by interlayer sliding, and the BSFV is thus feasible in both square and hexagonal lattices. The required stacking operations for achieving valley polarizations in all square and hexagonal lattices are listed in Tables S1 and S2 of the SM, respectively. Note that the operations to create bilayers include original stackings (direct stacking, rotation, mirror, etc.; see Tables S1 and S2) and sliding, where the BSFV with direct stacking and sliding is termed as sliding ferrovalley, analogous to sliding ferroelectricity [36–47]. As we will see, such BSFV strategy leads to many ferrovalley candidates. Noteworthy, both TR symmetry and SI symmetry can be kept with our BSFV strategy, in contrast to the previous strategies.

III. HIGH-THROUGHPUT SCREENING OF BSFV

We then work on a high-throughput screening to search monolayers that can realize BSFV. The screening of BSFV is conducted in three steps: (i) Start with the Computational 2D Materials Database [49,50] and find nonmagnetic monolayers, which possess bandgaps larger than 0.2 eV and exhibit thermal and dynamic stability. (ii) Then, select those with square or hexagonal lattices, i.e., layer group number being larger than 48. (iii) Lastly, examine the band structures and keep the systems that have either conduction band minimum (CBM) or valence band maximum (VBM) located at high-symmetry points or lines (excluding TR preserved Γ, M, K, K'). Such screening results in 352 valley materials, among which 14 exhibit direct bandgaps. All 352 valley materials are listed in Tables S3 and S4 of the SM. Among these BSFV candidate materials, 107 materials have been successfully synthesized experimentally in bulk or thin films. In the following sections, we demonstrate BSFV with the example systems of hexagonal RhCl_3 and square InI ,

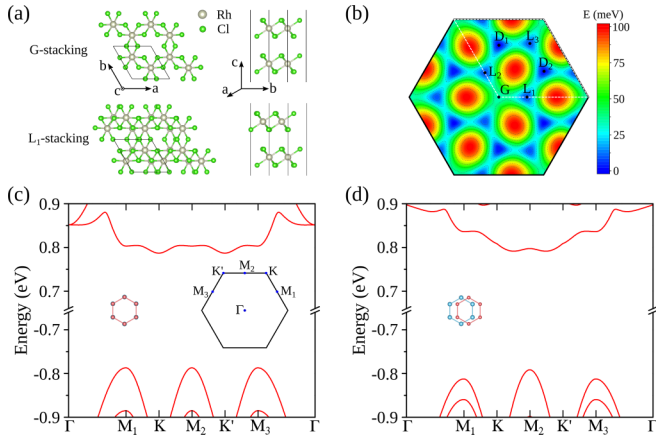


FIG. 2. Realizing BSFV in hexagonal RhCl₃. (a) Geometry of bilayer RhCl₃ with *G* and *L*₁ stackings. The left and right panels show the top and side views, respectively. (b) Energy landscape for different bilayer stackings. The white dotted parallelogram denotes the unit cell of monolayer. Points of *G*, *L*_{1/2/3}, and *D*_{1,2} represent stackings with fractional translations of (0,0), (1/3,0), (0,1/3), (2/3,2/3), (1/3,2/3), and (2/3,1/3), respectively. The ground states locate at *D*₁ and *D*₂ stackings, while *L*_{1/2/3} stackings are local minima. Panels (c) and (d) show band structures for *G* and *L*₁ stackings, respectively. The spin-orbit coupling is not considered for its negligible strength. The insets show high-symmetry points of the Brillouin zone, as well as the corresponding stackings.

which both exhibit direct bandgaps. Note that the BSFV concept also applies to these valley materials with indirect bandgaps, such as bilayer SnS₂, as detailed in the SM.

IV. BSFV IN HEXAGONAL-LATTICED RhCl₃

Bulk RhCl₃ is a van der Waals layered material within the *C*2/*m* space group, and has been experimentally synthesized at room temperature [61]. The cleavage energy of the RhCl₃ monolayer is 0.22 J/m² (see Fig. S2), which is smaller than that of graphene (0.46 J/m²) [62] and MoS₂ (0.42 J/m²) [63], indicating that RhCl₃ monolayer and multilayers can be obtained by mechanical exfoliation. Monolayer RhCl₃ crystallizes in honeycomb lattice with edge-sharing octahedra, which is similar to CrI₃. It belongs to the layer group of *p*3̄1*m* (No. 71) and the point group of *D*_{3*d*} [64]. The unit cell consists of two Rh and six Cl atoms, where the Rh atomic plane is sandwiched between two Cl atomic planes [see Fig. 2(a)]. The calculated phonons indicate that monolayer RhCl₃ is thermally stable and molecular dynamics simulation further confirms its being dynamically stable at room temperature (see Fig. S3 in the SM). The electronic band structure shows that the monolayer RhCl₃ has a direct bandgap of about 1.72 eV, with both the VBM and the CBM located at equivalent *M* points (see Fig. S4 in the SM). A triple degeneracy of valleys occurs at the *M*₁, *M*₂, and *M*₃ points, arising from the *C*_{3*z*} rotational symmetry. Therefore, it is legitimate to expect the bilayer RhCl₃ to be a good candidate for realizing BSFV.

Let us first determine the energy landscape of bilayer RhCl₃ with respect to sliding. We start with the so-called AA-stacked bilayer RhCl₃, which comes from directly stacking two monolayers, indicating that the possible BSFV here is

more precisely sliding ferrovalley. Note that Table S2 indicates that another stacking, where the top layer is flipped with respect to the AA stacking, is also possible to realize polarization, while it is not studied here since the valley polarized state is found to be energetically unfavorable. Here we adopt the following convention to consider sliding: the bottom layer is kept static, while the sliding amount of the top layer is described by $ma_1 + na_2$, where a_1 and a_2 are the lattice vectors, and (m , n) is a pair of fractional numbers that represent the sliding. The total energy as a function of sliding is obtained from density functional theory (DFT) calculations. As shown in Fig. 2(b), the sliding of *D*₁ (1/3,2/3) and *D*₂ (2/3,1/3) results in an energy doublet, which corresponds to the global minima, while the sliding of *L*₁ (1/3,0), *L*₂ (0,1/3), and *L*₃ (2/3,2/3) leads to an energy triplet that is local minima. The energy difference between such local and global minima is 2 meV/Rh.

We now examine the existence of BSFV in bilayer RhCl₃. Symmetry analysis on bilayer RhCl₃ indicates that the stackings of *G* and *D*_{1/2} all have *C*_{3*z*} symmetry, while the *L*_{1/2/3} stackings do not preserve the *C*_{3*z*} symmetry (see Table S2), which is consistent with the energy landscape [see Fig. 2(b)]. Therefore, valley polarization can be expected at *L*_{1/2/3} stackings, while not at *G* and *D*_{1/2} stackings. The band structures of bilayer RhCl₃ at *G* and *L*₁ stackings are obtained from DFT calculations, as shown in Figs. 2(c) and 2(d). Band structures of all other stackings are shown in Fig. S5. Here, we focus on the band dispersion of the valley at the *M*₁, *M*₂, and *M*₃ points. For the case of *G* stacking, the valleys at the *M*₁, *M*₂, and *M*₃ points are equivalent, as shown in Fig. 2(c). The band gap of bilayer RhCl₃ yields 1.57 eV, which indeed is similar with the value (1.72 eV) of monolayer. With a sliding of (1/3,0) to *L*₁ stacking, as expected, the energy degeneracy at *M*_{1/2/3} points is lifted, resulting in that the valley at the *M*₂ point becomes different from those at the *M*_{1/3} points, as shown in Fig. 2(d). Let us define valley polarization as $\Delta^v = E_{M_2}^v - E_{M_{1/3}}^v$ and $\Delta^c = E_{M_2}^c - E_{M_{1/3}}^c$, where *v* and *c* denote the valence band and conduction band, respectively, and *M*_{*i*} represents the valley index. It yields that $\Delta^v = 39$ meV and $\Delta^c = 22$ meV, which are significant and comparable to the Δ^v of established valley systems, such as VSe₂ (78 meV) [25], LaBr₂ (33 meV) [26], and VSi₂N₄ (63 meV) [28]. Note that, for *L*₁ stacking, the valleys at the *M*₁ and *M*₃ points remain equivalent, as guaranteed by the *m*₁₀₀ mirror symmetry. Such degeneracy between *M*₁ and *M*₃ points can also be removed by breaking the *m*₁₀₀ symmetry, e.g., with (1/6,1/3) sliding (see Fig. S6). Moreover, valley polarizations at the *M*₁ and *M*₃ points can be realized with sliding to *L*₂ (0,1/3) and *L*₃ (2/3,2/3), respectively (see Fig. S5). We further investigate the influence of substrates on the BSFV in the RhCl₃ bilayers. We chose h-BN as the substrate to construct the heterojunction of bilayers RhCl₃/h-BN, due to its widespread application as a capping layer in devices. Our results indicate that the influence of the h-BN on the band structure of bilayer RhCl₃ is negligible due to the weak coupling with substrate/cap layer (see Figs. S8 and S9).

Another important feature of the BSFV system is the valley polarization can be easily switched by interlayer sliding. Specifically, sliding from *G* stacking to *L*_{1/2/3} stackings does

not need to overcome any energy barrier, and the transition barrier among different $L_{1/2/3}$ points is found to be as low as 6 meV/Ru, when the sliding passes through a bridging $D_{1/2}$ point (see Fig. S7 in the SM). Moreover, the valley polarized states at $L_{1/2/3}$ stackings are found to be stable as they correspond to local energy minima. Such results indicate that the switching among the valley polarization states L_1 , L_2 , and L_3 can be easily achieved. Furthermore, valley-dependent optical selection rules exist in RhCl_3 bilayers (see Sec. 9 of the SM). Essentially, this means that we have the capability to selectively excite electrons from the VBM to the CBM in each valley by using linearly polarized light in a specific direction and given frequency. The presence of these optical selections makes RhCl_3 bilayers possible for applications in polarizers [31] and exciton valleytronics [16,32,33]. Such selection rules for RhCl_3 are thus different from the valley selectivity of the circularly polarized optical proposed in transition metal dichalcogenides [10–12]. Until here, we have demonstrated that BSFV is feasible and can be realized in bilayer RhCl_3 .

V. BSFV IN SQUARE-LATTICED InI

We further verify the BSFV theory within a square lattice, as exemplified by InI. Bulk InI is an experimentally synthesized layered semiconductor [65,66]. Recent theoretical studies demonstrate that monolayer and few-layer InI are also stable [67,68]. The calculated cleavage energy of InI monolayer is 0.35 J/m^2 (see Fig. S2 in the SM), which is also small enough for the mechanical exfoliation. Monolayer InI belongs to layer group $p4/nmm$ (No. 64) and point group D_{4h} . Band structure from DFT calculations shows that monolayer InI possesses degenerate valleys, which are connected by the fourfold rotational symmetry, along the Γ -X and Γ -Y paths (see Fig. S10). According to the group theory analysis (see Table S1), with direct AA stacking, the C_{4z} rotational symmetry can be broken by interlayer sliding, indicating a possible sliding ferrovalley system. The energy landscape of InI bilayers indicate that $N_1(1/2, 0)$ and $N_2(0, 1/2)$ stackings are the ground state, while the AA-stacked bilayer (G stacking) corresponds to a local minimum with an energy of 33 meV/In [see Fig. 3(b)]. As shown in Figs. 3(c) and 3(d), the valleys are degenerate at G stacking, while the degeneracy is lifted by $N_1(1/2, 0)$ and $N_2(0, 1/2)$ stackings, yielding valley polarization of $\Delta^c = 326 \text{ meV}$ [see Figs. 3(b), 3(d), and S11]. Such a large value is comparable to that induced by ferroelectricity in monolayer group-IV monochalcogenides [31]. Figure 2(b) shows that the energy barrier from N_1 directly to N_2 is 25 meV/In, indicating feasible switching (see Fig. S12). Similar to RhCl_3 bilayer, InI bilayers also have a valley-dependent optical selection rule, that is, at the Γ -X (Γ -Y) valley, the optical transition from VBM to CBM could only be excited by x -linearly (y -linearly) polarized light [see Sec. 9 of the SM]. Such selection is similar to the 2D ferroelectric GeSe in rectangular lattice [31]. Again, BSFV theory is demonstrated in InI.

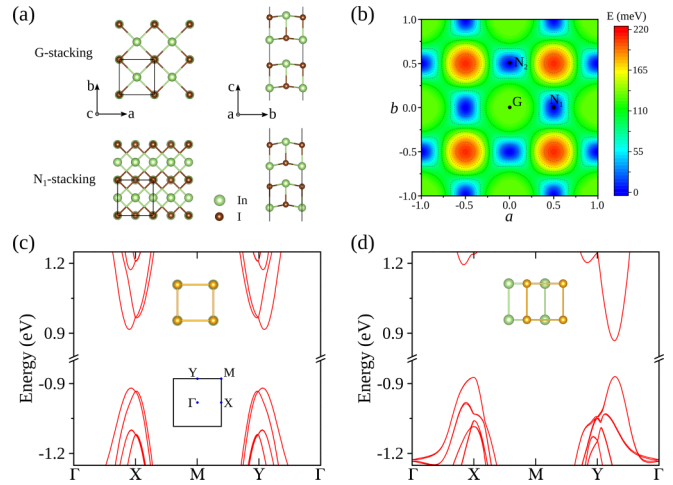


FIG. 3. Realizing BSFV in square InI. (a) Geometry of bilayer InI with G and N_1 stackings. The left and right panels show the top and side views, respectively. (b) Energy landscape for different bilayer stackings. Points of G and $N_{1,2}$ represent stackings with fractional translations of $(0,0)$, $(1/2,0)$, and $(0,1/2)$, respectively. The ground states locate at N_1 and N_2 stackings, while G stacking is a local minimum. Panels (c) and (d) show band structures for G and N_1 stackings, respectively. The spin-orbit coupling effect is not negligible, thus is considered here. The insets show high-symmetry points of the Brillouin zone, as well as the corresponding stackings.

In summary, we develop the BSFV theory, which is based on breaking of rotational symmetry and is thus irrelevant with TR and SI symmetries. Such an approach naturally leads to many ferrovalley candidates that can operate at room temperature. Our group theory analysis exhausts all possibilities, with which one only needs to know the layer group of a certain monolayer to tell whether the symmetry of the corresponding bilayer is compatible with BSFV. Combing high-throughput screening and DFT calculations, the sliding ferrovalley, which is a specific case of BSFV, is demonstrated in hexagonal RhCl_3 bilayer and square InI bilayer, both of which are nonmagnetic and nonferroelectric. Our BSFV theory thus expands the scope of ferrovalley systems and is likely to result in diverse applications of polarizers and exciton valleytronics.

ACKNOWLEDGMENTS

We acknowledge financial support from the Ministry of Science and Technology of the People's Republic of China (Grant No. 2022YFA1402901), NSFC (Grants No. 11825403, No. 11991061, and No. 12188101), the Guangdong Major Project of the Basic and Applied Basic Research (Future functional materials under extreme conditions—2021B0301030005), and the Shanghai Pilot Program for Basic Research, FuDan University 21TQ1400100 (23TQ017). C.X. also acknowledges support from NSFC (Grant No. 12274082), Shanghai Science and Technology Committee (Grant No. 23ZR1406600), and the open project of Guangdong Provincial Key Laboratory of Magnetoelectric Physics and Devices (Grant No. 2022B1212010008).

- [1] O. Gunawan, Y. P. Shkolnikov, K. Vakili, T. Gokmen, E. P. De Poortere, and M. Shayegan, Valley susceptibility of an interacting two-dimensional electron system, *Phys. Rev. Lett.* **97**, 186404 (2006).
- [2] D. Xiao, W. Yao, and Q. Niu, Valley-contrasting physics in graphene: Magnetic moment and topological transport, *Phys. Rev. Lett.* **99**, 236809 (2007).
- [3] A. Rycerz, J. Tworzydło, and C. W. J. Beenakker, Valley filter and valley valve in graphene, *Nat. Phys.* **3**, 172 (2007).
- [4] J. R. Schaibley, H. Y. Yu, G. Clark, P. Rivera, J. S. Ross, K. L. Seyler, W. Yao, and X. D. Xu, Valleytronics in 2D materials, *Nat. Rev. Mater.* **1**, 16055 (2016).
- [5] S. A. Vitale, D. Nezhich, J. O. Varghese, P. Kim, N. Gedik, P. Jarillo-Herrero, D. Xiao, and M. Rothschild, Valleytronics: Opportunities, challenges, and paths forward, *Small* **14**, 1801483 (2018).
- [6] D. Xiao, G. B. Liu, W. Feng, X. Xu, and W. Yao, Coupled spin and valley physics in monolayers of MoS₂ and other group-VI dichalcogenides, *Phys. Rev. Lett.* **108**, 196802 (2012).
- [7] P. San-Jose, E. Prada, E. McCann, and H. Schomerus, Pseudospin valve in bilayer graphene: Towards graphene-based pseudospintronics, *Phys. Rev. Lett.* **102**, 247204 (2009).
- [8] T. Cao, G. Wang, W. Han, H. Ye, C. Zhu, J. Shi, Q. Niu, P. Tan, E. Wang, B. Liu, and J. Feng, Valley-selective circular dichroism of monolayer molybdenum disulphide, *Nat. Commun.* **3**, 887 (2012).
- [9] X. Xu, W. Yao, D. Xiao, and T. F. Heinz, Spin and pseudospins in layered transition metal dichalcogenides, *Nat. Phys.* **10**, 343 (2014).
- [10] K. F. Mak, K. He, J. Shan, and T. F. Heinz, Control of valley polarization in monolayer MoS₂ by optical helicity, *Nat. Nanotechnol.* **7**, 494 (2012).
- [11] H. Zeng, J. Dai, W. Yao, D. Xiao, and X. Cui, Valley polarization in MoS₂ monolayers by optical pumping, *Nat. Nanotechnol.* **7**, 490 (2012).
- [12] W. T. Hsu, Y. L. Chen, C. H. Chen, P. S. Liu, T. H. Hou, L. J. Li, and W. H. Chang, Optically initialized robust valley-polarized holes in monolayer WSe₂, *Nat. Commun.* **6**, 8963 (2015).
- [13] Y. Li, J. Ludwig, T. Low, A. Chernikov, X. Cui, G. Arefe, Y. D. Kim, A. M. van der Zande, A. Rigosi, H. M. Hill *et al.*, Valley splitting and polarization by the Zeeman effect in monolayer MoSe₂, *Phys. Rev. Lett.* **113**, 266804 (2014).
- [14] A. Srivastava, M. Sidler, A. V. Allain, D. S. Lembke, A. Kis, and A. Imamoglu, Valley Zeeman effect in elementary optical excitations of monolayer WSe₂, *Nat. Phys.* **11**, 141 (2015).
- [15] G. Aivazian, Zhirui Gong, Aaron M. Jones, R.-L. Chu, J. Yan, D. G. Mandrus, C. Zhang, D. Cobden, W. Yao, and X. Xu, Magnetic control of valley pseudospin in monolayer WSe₂, *Nat. Phys.* **11**, 148 (2015).
- [16] Z. M. Yu, S. Guan, X. L. Sheng, W. Gao, and S. A. Yang, Valley-layer coupling: A new design principle for valleytronics, *Phys. Rev. Lett.* **124**, 037701 (2020).
- [17] J. Qi, X. Li, Q. Niu, and J. Feng, Giant and tunable valley degeneracy splitting in MoTe₂, *Phys. Rev. B* **92**, 121403(R) (2015).
- [18] Q. Zhang, S. A. Yang, W. Mi, Y. Cheng, and U. Schwingenschlogl, Large spin-valley polarization in monolayer MoTe₂ on top of EuO(111), *Adv. Mater.* **28**, 959 (2016).
- [19] C. Zhao, T. Norden, P. Zhang, P. Zhao, Y. Cheng, F. Sun, J. P. Parry, P. Taheri, J. Wang, Y. Yang, T. Scrace, K. Kang, S. Yang, G. X. Miao, R. Sabirianov, G. Kioseoglou, W. Huang, A. Petrou, and H. Zeng, Enhanced valley splitting in monolayer WSe₂ due to magnetic exchange field, *Nat. Nanotechnol.* **12**, 757 (2017).
- [20] D. Zhong, K. L. Seyler, X. Y. Linpeng, R. Cheng, N. Sivadas, B. Huang, E. Schmidgall, T. Taniguchi, K. Watanabe, M. A. McGuire, W. Yao, D. Xiao, K.-M. C. Fu, and X. Xu, Van der Waals engineering of ferromagnetic semiconductor heterostructures for spin and valleytronics, *Sci. Adv.* **3**, e1603113 (2017).
- [21] K. L. Seyler, D. Zhong, B. Huang, X. Linpeng, N. P. Wilson, T. Taniguchi, K. Watanabe, W. Yao, D. Xiao, M. A. McGuire *et al.*, Valley manipulation by optically tuning the magnetic proximity effect in WSe₂/CrI₃ heterostructures, *Nano Lett.* **18**, 3823 (2018).
- [22] T. Norden, C. Zhao, P. Zhang, R. Sabirianov, A. Petrou, and H. Zeng, Giant valley splitting in monolayer WS₂ by magnetic proximity effect, *Nat. Commun.* **10**, 4163 (2019).
- [23] A. Zhang, Z. Gong, Z. Zhu, A. Pan, and M. Chen, Effects of the substrate-surface reconstruction and orientation on the spin valley polarization in MoTe₂/EuO, *Phys. Rev. B* **102**, 155413 (2020).
- [24] A. Zhang, K. Yang, Y. Zhang, A. Pan, and M. Chen, Electrically switchable valley polarization, spin/valley filter, and valve effects in transition-metal dichalcogenide monolayers interfaced with two-dimensional ferromagnetic semiconductors, *Phys. Rev. B* **104**, L201403 (2021).
- [25] W. Y. Tong, S. J. Gong, X. Wan, and C. G. Duan, Concepts of ferrovalley material and anomalous valley Hall effect, *Nat. Commun.* **7**, 13612 (2016).
- [26] P. Zhao, Y. Ma, C. Lei, H. Wang, B. Huang, and Y. Dai, Single-layer LaBr₂: Two-dimensional valleytronic semiconductor with spontaneous spin and valley polarizations, *Appl. Phys. Lett.* **115**, 261605 (2019).
- [27] H.-X. Cheng, J. Zhou, W. Ji, Y.-N. Zhang, and Y.-P. Feng, Two-dimensional intrinsic ferrovalley GdI₂ with large valley polarization, *Phys. Rev. B* **103**, 125121 (2021).
- [28] Q. Cui, Y. Zhu, J. Liang, P. Cui, and H. Yang, Spin-valley coupling in a two-dimensional VSi₂N₄ monolayer, *Phys. Rev. B* **103**, 085421 (2021).
- [29] H. Y. Ma, M. Hu, N. Li, J. Liu, W. Yao, J. F. Jia, and J. Liu, Multifunctional antiferromagnetic materials with giant piezomagnetism and noncollinear spin current, *Nat. Commun.* **12**, 2846 (2021).
- [30] B. Wang, X. Zhang, Y. Zhang, S. Yuan, Y. Guo, S. Dong, and J. Wang, Prediction of a two-dimensional high-*T_C* f-electron ferromagnetic semiconductor, *Mater. Horiz.* **7**, 1623 (2020).
- [31] X.-W. Shen, W.-Y. Tong, S.-J. Gong, and C.-G. Duan, Electrically tunable polarizer based on 2D orthorhombic ferrovalley materials, *2D Mater.* **5**, 011001 (2017).
- [32] Y. Wang, W. Wei, F. Li, X. Lv, B. Huang, and Y. Dai, Valley polarization caused by crystalline symmetry breaking, *Mater. Horiz.* **8**, 244 (2021).
- [33] Y. Xu, Y. Wang, S. Wang, S. Yu, B. Huang, Y. Dai, and W. Wei, Spontaneous valley polarization caused by crystalline symmetry breaking in nonmagnetic LaOMX₂ monolayers, *Nano Lett.* **22**, 9147 (2022).
- [34] C. Wang, L. You, D. Cobden, and J. Wang, Towards two-dimensional van der Waals ferroelectrics, *Nat. Mater.* **22**, 542 (2023).

- [35] Y. Cao, V. Fatemi, S. Fang, K. Watanabe, T. Taniguchi, E. Kaxiras, and P. Jarillo-Herrero, Unconventional superconductivity in magic-angle graphene superlattices, *Nature (London)* **556**, 43 (2018).
- [36] L. Li and M. Wu, Binary compound bilayer and multilayer with vertical polarizations: Two-dimensional ferroelectrics, multiferroics, and nanogenerators, *ACS Nano* **11**, 6382 (2017).
- [37] J. Xiao, Y. Wang, H. Wang, C. D. Pemmaraju, S. Wang, P. Muscher, E. J. Sie, C. M. Nyby, T. P. Devereaux, X. Qian *et al.*, Berry curvature memory through electrically driven stacking transitions, *Nat. Phys.* **16**, 1028 (2020).
- [38] K. Yasuda, X. Wang, K. Watanabe, T. Taniguchi, and P. Jarillo-Herrero, Stacking-engineered ferroelectricity in bilayer boron nitride, *Science* **372**, 1458 (2021).
- [39] M. Vizner Stern, Y. Waschitz, W. Cao, I. Nevo, K. Watanabe, T. Taniguchi, E. Sela, M. Urbakh, O. Hod, and M. Ben Shalom, Interfacial ferroelectricity by van der Waals sliding, *Science* **372**, 1462 (2021).
- [40] Y. Wan, T. Hu, X. Mao, J. Fu, K. Yuan, Y. Song, X. Gan, X. Xu, M. Xue, X. Cheng *et al.*, Room-temperature ferroelectricity in $1T'$ -ReS₂ multilayers, *Phys. Rev. Lett.* **128**, 067601 (2022).
- [41] P. Meng, Y. Wu, R. Bian, E. Pan, B. Dong, X. Zhao, J. Chen, L. Wu, Y. Sun, Q. Fu *et al.*, Sliding induced multiple polarization states in two-dimensional ferroelectrics, *Nat. Commun.* **13**, 7696 (2022).
- [42] J. Ji, G. Yu, C. Xu, and H. J. Xiang, General theory for bilayer stacking ferroelectricity, *Phys. Rev. Lett.* **130**, 146801 (2023).
- [43] W. Li, X. Zhang, J. Yang, S. Zhou, C. Song, P. Cheng, Y. Q. Zhang, B. Feng, Z. Wang, Y. Lu *et al.*, Emergence of ferroelectricity in a nonferroelectric monolayer, *Nat. Commun.* **14**, 2757 (2023).
- [44] L. P. Miao, N. Ding, N. Wang, C. Shi, H. Y. Ye, L. Li, Y. F. Yao, S. Dong, and Y. Zhang, Direct observation of geometric and sliding ferroelectricity in an amphidynamic crystal, *Nat. Mater.* **21**, 1158 (2022).
- [45] F. Sui, M. Jin, Y. Zhang, R. Qi, Y. N. Wu, R. Huang, F. Yue, and J. Chu, Sliding ferroelectricity in van der Waals layered γ -InSe semiconductor, *Nat. Commun.* **14**, 36 (2023).
- [46] X. Wang, K. Yasuda, Y. Zhang, S. Liu, K. Watanabe, T. Taniguchi, J. Hone, L. Fu, and P. Jarillo-Herrero, Interfacial ferroelectricity in rhombohedral-stacked bilayer transition metal dichalcogenides, *Nat. Nanotechnol.* **17**, 367 (2022).
- [47] L. Yang and M. Wu, Across-layer sliding ferroelectricity in 2D heterolayers, *Adv. Funct. Mater.* **33**, 2301105 (2023).
- [48] See Supplemental Material at <http://link.aps.org/supplemental/10.1103/PhysRevB.109.075434> for detailed group theory analysis of BSFV; BSFV candidate materials by high-throughput search; details of first-principles calculation; BSFV in RhCl₃, InI, and SnS₂; and optical selection rule, and which includes Refs. [49–60].
- [49] S. Hastrup, M. Strange, M. Pandey, T. Deilmann, P. S. Schmidt, N. F. Hinsche, M. N. Gjerding, D. Torelli, P. M. Larsen, A. C. Riis-Jensen *et al.*, The Computational 2D Materials Database: High-throughput modeling and discovery of atomically thin crystals, *2D Mater.* **5**, 042002 (2018).
- [50] M. N. Gjerding, A. Taghizadeh, A. Rasmussen, S. Ali, F. Bertoldo, T. Deilmann, N. R. Knøsgaard, M. Kruse, A. H. Larsen, S. Manti *et al.*, Recent progress of the Computational 2D Materials Database (C2DB), *2D Mater.* **8**, 044002 (2021).
- [51] G. Kresse and J. Furthmüller, Efficient iterative schemes for *ab initio* total-energy calculations using a plane-wave basis set, *Phys. Rev. B* **54**, 11169 (1996).
- [52] P. E. Blöchl, Projector augmented-wave method, *Phys. Rev. B* **50**, 17953 (1994).
- [53] G. Kresse and D. Joubert, From ultrasoft pseudopotentials to the projector augmented-wave method, *Phys. Rev. B* **59**, 1758 (1999).
- [54] S. Grimme, J. Antony, S. Ehrlich, and H. Krieg, A consistent and accurate *ab initio* parametrization of density functional dispersion correction (DFT-D) for the 94 elements H-Pu, *J. Chem. Phys.* **132**, 154104 (2010).
- [55] G. Henkelman, B. P. Uberuaga, and H. Jónsson, A climbing image nudged elastic band method for finding saddle points and minimum energy paths, *J. Chem. Phys.* **113**, 9901 (2000).
- [56] M. X. Chen and M. Weinert, Revealing the substrate origin of the linear dispersion of silicene/Ag, *Nano Lett.* **14**, 5189 (2014).
- [57] M. Chen and M. Weinert, Layer *k*-projection and unfolding electronic bands at interfaces, *Phys. Rev. B* **98**, 245421 (2018).
- [58] A. Togo and I. Tanaka, First principles phonon calculations in materials science, *Scr. Mater.* **108**, 1 (2015).
- [59] M. S. Dresselhaus, G. Dresselhaus, and A. Jorio, *Group Theory: Application to the Physics of Condensed Matter* (Springer Science & Business Media, Berlin, 2007).
- [60] F. Lou, X. Li, J. Ji, H. Yu, J. Feng, X. Gong, and H. Xiang, PASP: Property analysis and simulation package for materials, *J. Chem. Phys.* **154**, 114103 (2021).
- [61] H. Bärnighausen and B. K. Handa, Die kristallstruktur von rhodium(III)-chlorid, *J. Less-Common Met.* **6**, 226 (1964).
- [62] W. Wang, S. Dai, X. Li, J. Yang, D. J. Srolovitz, and Q. Zheng, Measurement of the cleavage energy of graphite, *Nat. Commun.* **6**, 7853 (2015).
- [63] T. Bjorkman, A. Gulans, A. V. Krasheninnikov, and R. M. Nieminen, van der Waals bonding in layered compounds from advanced density-functional first-principles calculations, *Phys. Rev. Lett.* **108**, 235502 (2012).
- [64] Y. Kadioglu, I. Ozdemir, O. U. Akturk, G. Gokoglu, U. Akinci, and E. Akturk, Tuning the electronic structure of RhX₃ (X = Cl, Br, I) nonmagnetic monolayers: Effects of charge-injection and external strain, *Phys. Chem. Chem. Phys.* **22**, 4561 (2020).
- [65] A. Bach, D. Fischer, and M. Jansen, Metastable phase formation of indium monochloride from an amorphous feedstock, *Z. Anorg. Allg. Chem.* **639**, 465 (2013).
- [66] W. A. Dunlap-Shohl, I. G. Hill, Y. Yan, and D. B. Mitzi, Photovoltaic effect in indium(I) iodide thin films, *Chem. Mater.* **30**, 8226 (2018).
- [67] J. Wang, B. Dong, H. Guo, T. Yang, Z. Zhu, G. Hu, R. Saito, and Z. Zhang, Stability and electronic properties of two-dimensional indium iodide, *Phys. Rev. B* **95**, 045404 (2017).
- [68] Z. Ma, F. Wu, Y. Liu, and E. Kan, Giant band gap reduction and insulator–metal transition in two-dimensional InX (X = Cl, Br, I) layers, *J. Phys. Chem. C* **123**, 21763 (2019).